Article

Ingenious design of DNA concatamers and G-quadruplex wires assisted assembly of multi-branched DNA nanoarchitectures for ultrasensitive biosensing of miRNA

Jianguo Xu, Chao Yan, Xinxin Wang, Bangben Yao, Jian-feng Lu, Guodong Liu, and Wei Chen

Anal. Chem., **Just Accepted Manuscript** • DOI: 10.1021/acs.analchem.9b01353 • Publication Date (Web): 25 Jun 2019

Ingenious design of DNA concatamers and G-quadruplex wires assisted assembly of multi-branched DNA nanoarchitectures for ultrasensitive biosensing of miRNA

Jianguo Xu[1,†], Chao Yan[1, 2,†], Xinxin Wang[1], Bangben Yao[3], Jianfeng Lu[1], Guodong Liu[2, 4,*], Wei Chen[1,*]

[1]Engineering Research Center of Bio-process, MOE, School of Food and Biological Engineering, Hefei University of Technology, Hefei 230009, P. R. China
[2]Research Center for Biomedical and Health Science, School of Life and Health, Anhui Science & Technology University, Fengyang, 233100, China
[3]Anhui Province Institute of Product Quality Supervision & Inspection, Hefei, 230051, P.R. China
[4]Department of Chemistry and Biochemistry, North Dakota State University, Fargo, North Dakota, 58105, US

*Correspondence should be addressed to Dr. & Prof. Wei Chen & Guodong Liu. Email: chenweishnu@163.com, guodong.liu@ndsu.edu

†These two authors contributed equally to this research.

* Corresponding e-mail: chenweishnu@163.com; guodong.liu@ndsu.edu

Abstract

Facile and efficient assembly of intelligent DNA nano-objects with the ability to exert robust microRNAs determination is essential for DNA nanobiotechnology and basic biomedical study. Herein, we presented a novel target-triggered DNA assembly pathway for the construction of multi-branched DNA nanoarchitectures by the combination of DNA concatamers with G-quadruplex wires. The DNA concatamers acting as the main body structures were assembled by hybridization chain reaction (HCR), while the G-quadruplex wires acting as the branch structures were generated by terminal deoxynucleotidyl transferase (TdT)-promoted polymerization and G-quadruplex units (GUs) based self-assembly. With copious number of G-quadruplex replicates collected on the electrode surface, the obtained multi-branched DNA nanoarchitectures were able to bind with lots of hemin, which further led to a significantly amplified electrochemical sensing signal for ultrasensitive and selective detection of miRNA-21. The detection limit was achieved as low as 0.2 fM with a wide dynamic response ranging from 10 fM to 100 nM, which is much powerful or at least comparable to most of the reported studies. Furthermore, the electrochemical biosensor offered an excellent specificity and even the single-base mutation against the perfectly-matched target miRNA can be easily distinguished easily. Furthermore, the real biological samples were also desirably analyzed, indicating the proposed strategy an ideal platform for the fabrication of versatile DNA nano-biosensors.

Keywords: DNA concatamer, G-quadruplex wire, multi-branched DNA nanoarchitectures, microRNA determination, electrochemical sensing

Introduction

MicroRNAs (miRNAs) are a class of small endogenous noncoding RNAs (17-22 nucleotide) that act as key players across various biological processes such as gene expression, cell cycle, and biology development[1]. Over the past two decades, the miRNAs biology field has expanded widely and related fundamental studies have revealed that miRNAs alterations can contribute to many cases of diseases, in particular, human cancer development and progression with miRNAs acting as tumor suppressors or oncogenes. And, these miRNAs may become a new branch of potential biomarkers in early tumor diagnosis and clinical management[2,3]. Therefore, accurate miRNAs profiling holds considerable prospect for further understanding miRNAs functions, as well as reducing the morbidity and mortality of cancer.

Conventional approaches such as quantitative reverse transcriptase-polymerase chain reaction (qRT-PCR)[4], northern blotting[5], and microarray[6,7] have been previously developed for successful detection of miRNAs with considerable improvements. However, these prominent strategies still undergo regrettable defects for miRNA assays. The qRT-PCR technique is usually time-consuming and highly depended to thermostable enzymes. The northern blotting techniques have a high risk of cross contaminations and operational complexity. The low sensitivity and poor specificity are also the unsolved issues of microarray-based methods. Additionally, the inherent characteristics of miRNAs including their small sizes, extremely low expression levels in total RNA samples, high sequence homology among family members, and susceptibility to degradation have strongly restricted the direct miRNAs analysis.

Accordingly, quantitative and qualitative detection of trace microRNAs is extremely important to decipher the role of miRNAs in clinical diagnosis but remains a great challenge[8].

Advances in molecule biology have led to deep understanding of nucleic acids that they can not only be used for storing of genetic information but can also perform defined functions such as the assembly scaffold since the predictable, programmable, and controllable nature of Watson-Crick base-pairing rules[9,10] and the π-π stacking effect[11]. DNA concatamers, which are self-assembled into duplex helixes by a pair of short oligonucleotide strands through hybridization chain reaction (HCR)[12,13] have been frequently designed to develop direct signal amplification strategy towards the analysis of nucleic acid, protein and small molecules [14,15]. G-quadruplex, which is formed by the guanine-rich single-stranded oligonucleotide sequences in the presence of specific metal cations, were widely explored as the optical and electrochemical reporting unit to construct a variety of signal amplification methods for desired analysis[16-18]. Interestingly, recent studies have proved that the single small G-quadruplex unit (GU) can be able to spontaneously assemble into a highly ordered stiff G-quadruplex wire superstructure through π-π stacking[11,19]. And the randomly arrayed G-quadruplex wires can also be generated by the specific template-free polymerase of terminal deoxynucletidyl transferase (TdT)[20], which can catalyze the incorporation of deoxyguanosine triphosphate (dGTP) and deoxyadenosine triphosphate (dATP) into the 3'-OH terminus of single-stranded DNA strands[21,22] and consequently produce a long G-quadruplex tail. Heuristically, it is strategically conceived that the effective

combination of DNA concatamers and G-quadruplex wires will enhance the convenience of assembly and application of DNA nanoobjects for constructing new biosensing platforms and upgrading the biosensor performance.

Taken aforementioned into consideration, in this work, we presented a proof-of-concept electrochemical biosensor functionalized with the assembly of multi-branched DNA nanoarchitectures for miRNA-21 detection, which was treated as one of the representative biomarkers regulating all types of cancers[23]. There are two key parts of the assembled DNA nanoarchitectures: the main structure and the branch structure. The main structure of the DNA nanoarchitectures were DNA concatamers, which were constructed via the alternating hybridization between two ssDNA assembly probes. The branch structure of the DNA nanoarchitectures were G-quadruplex wires, which were constructed by both the TdT-promoted DNA elongation polymerization and GUs based self-assembly. In the presence of target miRNA-21, the DNA concatamers with plentiful exposed biotin sites at 5'-terminus would be successfully anchored on the electrode surface, which could be then act as the carrier to accumulate the G-quadruplex wire composed DNA branch structures via the specific recognition set of streptavidin and biotin. The resulting DNA nanoarchitectures could tightly bind with hemin for the detection of target miRNA-21 with the amplified current signals, and the current change was directly related to the miRNA-21 concentration.

Experimental

Reagents and chemicals

Tris (hydroxymethyl) aminomethane (Tris), dimethyl sulfoxide (DMSO), and ethylene diamine tetraacetic acid (EDTA) were obtained from Sinopharm Chemical Reagent Company (Shanghai, China). Tris (2-carboxyethyl) phosphine hydrochloride (TCEP), 6-Mercaptohexanol (MCH), TdT, dGTP, dATP, streptavidin (SAV), 4-(2-hydroxyethyl) piperazine-1 ethanesulfonic acid sodium salt (HEPES), and HPLC-purified oligonucleotides **(Table S1)** were purchased from Shanghai Sangon Biological Engineering Technology and Services Co. Ltd. (Shanghai, China). Hemin was provided by Aladdin Reagents (Shanghai, China) and dissolved in DMSO to prepare the stock solution (10 mM). The HEPES buffer (20 mM, pH 8.0) containing 50 mM KCl and 200 mM NaCl was used to dilute the stock solution of hemin. If there were no special descriptions, all other metal salt reagents, such as $K_3Fe[CN]_6$ and $K_4Fe[CN]_6$ et al. were all at the analytical grade and supplied by Sinopharm Chemical Reagent Company (Shanghai, China). Ultrapure water (Milli-A10 system, Millipore) with a resistivity of 18.2 MΩ/cm was used throughout the experiments. Tris-buffer (pH 7.4) containing 10 mM Tris, 100 mM NaCl, and 10 mM $MgCl_2$ was used for DNA hybridization. The tris (hydroxymethyl) aminomethane (Tris-HCl) buffer (pH= 8.0) containing 10 mM Tris and 1 mM EDTA was used for preparing the stock solutions of all oligonucleotides. The three-electrode system was adopted for the measurement in this research with the Au electrode as the working electrode, a platinum wire as the auxiliary electrode, and an Ag/AgCl as the reference electrode, respectively.

Pretreatment of Au electrode

In a typical procedure, the Au electrode (3 mm in diameter) was firstly polished with

the 0.05 μm alumina slurry on a flat pad for 5 min to obtain a mirror-like surface. After that, the Au electrode was soaked in an as-prepared piranha solution (H_2SO_4/H_2O_2, volume ratio 3:1) for 30 min, followed by a thorough rinse with ultrapure water and sonication with ethanol and ultrapure water for 5 min to remove any remaining impurities. Subsequently, the electrochemical cleaning of the electrode was carried out in 0.5 M H_2SO_4 solution by potential scanning between -0.2 and 1.5 V at a scan rate of 100 mV/s until remarkable voltammetric peaks were obtained. Finally, the electrode was rinsed with the ultrapure water and dried with the nitrogen current.

Fabrication of the electrochemical biosensor

Prior to the electrochemical detection, the DNA concatamers ($[AP1+AP2]_n$) and extended G-quadruplex wires should be constructed by HCR and TdT-promoted DNA polymerization, respectively. In a typical HCR, an Eppendorf tube containing 10 μL of Tris-buffer, 5 μL of 2 μM AP1, and 5 μL of 2 μM AP2 was heated at 95 ℃ for 5 min and then allowed to cool down to 37 ℃ to form the tandem sequence of $[AP1+AP2]_n$ for 0.5 h. The obtained DNA concatamers were directly used for the electrode surface assembly. The TdT-promoted DNA polymerization for G-quadruplex wires creation was adopted based on the reported method with a slight modification[20]. Briefly, 10 μL of the reaction mixture containing 5 μL of 2 μM EP, 2 μL of 10 mM dNTP (molar ratio of dGTP: dATP= 7: 3), and 1 μL of TdT (10 U) associated with its buffer (2 μL) was added into a 200 μL Eppendorf tube and kept at 37 °C for 1 h to implement the catalytic reaction. The resultant mixture was terminated by heating at 95 °C for 3 min and then incubated with HEPES to form the G-quadruplex wire. The concentration of obtained

G-quadruplex wire can be calculated from the EP concentration. In addition, the thiol-labelled CP was incubated with 1 mM TCEP for 0.5 h to reduce disulfide bonds at room temperature.

For electrochemical sensing interface fabrication, a droplet (7.5 μL) of activated CP was firstly placed on the Au working electrode and incubated at 4 ℃ for 12 h. Next, 5 μL of 1.0 mM MCH was casted on the electrode and incubated for 0.5 h to block the unoccupied sites and make the CPs linear, followed by addition of 5 μL of target miRNA-21 at different concentrations. Subsequently, the above already formed DNA concatamers (5 μL) were pipetted and incubated for 1 h on the electrode surface and further interacted with the SAV solution (5 μL, 10 ng/μL) for 15 min. The biotin-labeled G-quadruplex wire (5 μL, 1 μM) was then similarly dropped onto the electrode surface and allowed to react with SAV for another 15 min. Afterwards, the GU (5 μL) at the concentration of 1 μM was added to bind with the G-quadruplexes along the G-quadruplex wire for 1 h and to form more G-quadruplex wires with the aid of Mg^{2+}. Finally, the functionalized electrode was treated with 5 μL 0.2 mM hemin for 30 min to form the G-quadruplex/hemin complexes, which were ready for the electrochemical measurements. For the control experiments, the Au electrode was identically fabricated but without the involvement of interrogated elements, such as the target miRNA-21 or the signal amplification treatments.

Unless otherwise stated, the electrode surface at each modification procedure should be carefully and gently rinsed with the ultrapure water and dried with nitrogen stream to remove the excessive species.

Electrochemical measurements

All electrochemical measurements, including differential pulse voltammetry (DPV), cyclic voltammetry (CV), and electrochemical impedance spectroscopy (EIS) were performed on a CHI 660D electrochemical analyzer (Chenhua Instrument Company, Shanghai, China) at room temperature. A conventional three-electrode cell was employed with the Au electrode as the working electrode, a platinum wire as the auxiliary electrode, and an Ag/AgCl as the reference electrode. CV scan was performed in 5 mM $[Fe(CN)_6]^{3-/4-}$ (containing 0.1 M KCl) with a 50 mV/s scan rate from -0.2 to 0.6 V. Electrochemical impedance spectroscopy (EIS) was measured in 5 mM $[Fe(CN)_6]^{3-/4-}$ (containing 0.1 M KCl) with the frequency range from 10 kHz to 0.1 Hz. DPV measurement was recorded in 20 mM HEPES solution (50 mM KCl, 200 mM NaCl, pH 8.0) with the pulse amplitude and period of 50 mV and 50 ms, respectively. Notably, the HEPES solution should be thoroughly degassed under the stream of nitrogen for 30 min before usage.

Native polyacrylamide gel electrophoresis (Native-PAGE) analysis of the assembled DNA structure

To prepare the hydrogel, 6 mL 40 % gel solution (39:1), 3 mL 5× TBE Buffer, 110 μL 10 % ammonium persulfate APS, 10 μL TEMED and 5.9 mL deionized water were thoroughly mixed to proceed the polymerization at room temperature for about 30 min. This obtained mixture contained a final gel percentage of 12 %. The electrophoretic samples were prepared by mixing 10 μL of the oligonucleotide solution, 1.5 μL of the 6× loading buffer, and 1 μL of the nucleic acid dye (10× SYBR Green I) together, which

were then subjected to the 12 % native-PAGE on an electrophoresis cell (Bio-Rad) by using 1× TBE as the running buffer. The electrophoresis was conducted at 80 V constant voltage for 1.5 h. Obtained gel images were scanned using a Gel Imaging System (Shanghai, China).

Results and discussion

Principle of the electrochemical biosensor

In the present work, the DNA concatamers were integrated with G-quadruplex wires for efficiently assembling into the multi-branched DNA nanoarchitectures to realize the robust and ultrasensitive electrochemical biosensing of miRNA. The DNA concatamers were constructed by HCR with the assembly scaffolds of AP1 and AP2 (**Figure S1**), and the extended G-quadruplex wires with numerous G-quadruplex repeats were yielded based on the TdT-promoted polymerization (**Figure S2**). Of note, the DNA concatamers were constructed by HCR in the homogeneous solution rather than on the surface of the electrode. The higher collision probability among the molecules induced higher reaction kinetics in the solution and the easy control of reaction conditions such as the annealing temperature are the two main reasons for the adoption of HCR in solution. **Figure 1** outlined the detailed assembly and construction process of the presented electrochemical biosensor. At the beginning, the thiol-modified CP with the complementary region towards target miRNA-21 was covalently conjugated onto the cleaned Au electrode surface via the classic Au-S bonds (step ①).Thereafter, MCH was used to block the remaining sites and stand up the CP to improve its hybridization

efficiency (step ②). In the presence of target analyte, the miRNA-21 was precisely recognized by CP, and a CP-miRNA duplex with a swing tail that complementary to AP1 at the 3' terminus of miRNA-21 was formed (step ③). On this basis, the main body structure of DNA concatamer with many biotins attached could be tightly dragged to the electrode surface through hybridization (step ④) and led to the further introduction of plentiful of streptavidin molecules by the specific recognition between streptavidin and biotin (step ⑤). Similarly, the biotin-tagged G-quadruplex wire could strongly conjugate with the main body structure (step ⑥). Considering that one streptavidin molecule was able to bind with four biotin molecules and one binding site of streptavidin was already occupied, the associated branch amount was about three times higher than that of the biotin. Subsequently, with the aid of Mg^{2+}, the introduced G-quadruplex wire could sever as the primary trigger to bind with abundant GUs, which could finally promote the direct growth of thousands of GUs into well-defined G-quadruplex wire superstructures and greatly increase the branch structure number through an uninterrupted π-π stacking system[11] (step ⑦). In this case, the multi-branched DNA nanoarchitectures composed by DNA concatamers and G-quadruplex wires were well fabricated. Upon addition of hemin (step ⑧), the specific interaction of G-quadruplex towards hemin led to the formation of G-quadruplex/hemin complexes, therapy creating significantly amplified quantitative electrochemical redox signals[20]. On the contrary, in the absence of target miRNA, the multi-branched DNA nanoarchitectures could not be formed onto the electrode surface to generate the electrochemical signal. As a result, the multi-branched DNA nanoarchitectures were

achieved in the designed model for ultrasensitive miRNA analysis.

Preferred position for **Figure 1**

Electrochemical characterization of fabricated DNA biosensor

To demonstrate the detection principle, the stepwise fabrication processes were characterized by recording the cyclic voltammogram (CV) and electrochemical impedance spectra (EIS) in 5 mM $[Fe(CN)_6]^{3-/4-}$ (containing 0.1 M KCl) as the electroactive probes. As shown in **Figure 2A**, a pair of well-defined redox peaks representing the high efficiency of the electron transfer ability were obviously observed with the bare Au electrode (curve a). After modification with CPs, it could be seen from curve b that the redox peak significantly decreased because of the formation of a negatively charged DNA monolayer on the electrode surface. The subsequent modification of blocking regent MCH covered the residual active sites, further inhabiting the electron transfer ability (curve c). When target miRNA-21 (curve d), DNA concatamers (curve e), extended G-quadruplex wires (curve f), and GUs (curve g) were introduced into the electrode surface in sequence, as expected, the electrostatic repulsion between $[Fe(CN)_6]^{3-/4-}$ and the negative charged DNA phosphate backbones prevented the diffusion of ferricyanide toward the electrode surface, leading to the decrease of redox peak current and the increase of peak-to-peak separation step-by-step.

Figure 2B was the Nyquist plot of the EIS corresponding to the modified electrode at different stages. The semicircle diameter at higher frequencies was equal to the

electron-transfer resistance (Ret), and the straight line was related to the diffusion process at low frequencies[24]. It can be found that the EIS of the bare electrode exhibited an almost straight line (curve a), suggesting the diffusion of $[Fe(CN)_6]^{3-/4-}$. Once the CPs were decorated via Au-S bond, the Ret was substantially increased given the negatively charged DNA phosphate backbone attenuated the electron transfer (curve b). With the participation of MCH to obstruct the electron transfer, the Ret was continually increased (curve c). Afterwards, the remaining target miRNA recognition (curve d), DNA concatamers combination (curve e), extended G-quadruplex wires interaction (curve f), and GUs assembly (curve g) made more and more phosphate backbone of the oligonucleotides attached, therapy producing an incremental electrostatic repulsion force to $[Fe(CN)_6]^{3-/4-}$. In consequence, the Ret values displayed with an increasing trend. These CV results and EIS changes of the electrode behavior are in good accordance with each other, and confirm the well modifications of the sensing interface, demonstrating that the electrochemical biosensor has been fabricated successfully according to **Figure 1**.

Preferred position for **Figure 2**

Sensing Feasibility investigation

To verify the feasibility, the DPV measurements were carried out to study the proposed strategy without/with GU in the absence /presence of target miRNA-21. As recorded in **Figure 3**, in the absence of target miRNA-21, no matter if the GU was involved (curve c) or not (curve a), the electrochemical background current response was very weak,

which was basically due to the highly minimized accumulation of hemin without the target conjugation. On the contrary, the introduction of target miRNA-21 into the interface construction induced a dramatically enhanced peak current in curve b and d. Such changes are mainly assigned to the plentiful collection of G-quadruplex DNA nanostructures responsible for binding with hemin to export greatly enhanced electrochemical signal. It should be noted that the amplified current response of curve d is higher than that of curve b since the final addition of GU could trigger the G-quadruplex wires formation and further increase the amount of associated hemin. Therefore, the provided comparative results confirm that the assembly of multi-branched DNA nanoarchitectures is available for amplified signaling of miRNA sensing.

Preferred position for **Figure 3**

Quantitative analysis of miRNA

Under optimized experimental conditions (**Figure S3**), the sensitivity and dynamic range were assessed by DPV measurements because of its higher sensitivity for the detection of redox probes with low concentrations. As described in **Figure 4A**, the oxidation peak current increased with the increase of miRNA-21 concentration ranging from 10 fM to 100 nM, indicating that the assembled multi-branched DNA nanoarchitectures were highly dependent on the concentration of miRNA-21. When the concentration of miRNA-21 was further increased, such as 500 nM, the limited amount of fixed CP for miRNA-21 recognition cannot induce obvious signal increase any more.

Figure 4B displayed the plot of the current signal (I) vs. the logarithm of miRNA-21 concentration. It was found that a good linear relationship (R^2= 0.9820) between the peak current I and logarithmic miRNA-21 concentration was achieved with a regression curve of Y= 176.8 lgX+ 1225.7, where Y and X represented current I and the miRNA-21 concentration, respectively. The linear range was from 10 fM to 100 nM, and the detection limit was calculated to be 0.2 fM on the basis of the 3 σ/slope (σ, standard deviation of the blank samples). These results indicate that the intelligently designed DNA superstructures assembly strategy can ensure an excellent sensitivity for miRNA detection. Compared to the existing biosensor methodologies for miRNA determinations (**Table S2**), the sensitivity and the dynamic range of our proposed strategy was at least 25-fold higher and 2 orders of amplitude wider than the literature values, respectively.

Preferred position for **Figure 4**

Actually, this strategy shows the following superior features that contribute to the desirable assay performance. First, the use of DNA concatamers as the main body structure confers the DNA nanoarchitectures with many sites for building branch structures; Second, the bridge function of streptavidin facilitates the further increase of the binding sites on DNA concatamers; Third, the high polymerization efficiency of TdT offers the branch structure of G-quadruplex wires with lots of G-quadruplex replicates; Forth, the GU self-growth on the G-quadruplex wires promote more G-quadruplex wires formed. In view of these advantages, the multi-branched DNA nanoarchitectures were capable of accumulating lots of hemin and in turn inducing

strikingly improved electrochemical signal to satisfy the requirement of trace biomarkers profiling.

Specificity study

For miRNA analysis, the mutation phenomenon severs as the crucial indicator for clinical diagnosis. In this section, the specificity was interrogated by comparative exploration of several control miRNAs, including the perfect-matched target miRNA (T), one-base mismatched miRNA (M1), two-base mismatched miRNA (M2), three-base mismatched miRNA (M3), inserted miRNA (IM), deleted miRNA (DM), and non-target miRNA (MiRNA-10b, MiRNA-141, MiRNA-200b, and Let-7d) under the same experimental procedures. A sample without target is selected as the blank control. As presented in **Figure 5**, by defining the net signal enhancement of T as 100 %, the relative signals responding to M1, M2, M3 were only about 37.3 %, 23.4 %, 17.7 %, respectively. And, the signals for IM, DM, and all non-targets were almost negligible. These inspiring results could be ascribed to the fact that the mismatched, inserted, deleted or non-target miRNAs have poor hybridization abilities with CP and the subsequent DNA concatamers, indicating the proposed biosensor holds an excellent specificity for miRNA detection even with one base mutation.

Preferred position for **Figure 5**

Real sample analysis

In order to evaluate the practical applicability of our electrochemical biosensor for real

biological samples detection, the cell lines of human cervical cancer (HeLa) and human breast cancer (MCF-7) expressed with miRNA-21 were selected to perform the real miRNA assay. The total RNA of Hela and MCF-7 were extracted by using an appropriate amount of Trizol reagent according to the indicated manufacturer instructions. As gathered in **Figure 6**, both the current signals produced by HeLa and MCF-7 can be well distinguished from the blank sample, and their signal responses increased with the increment of cell number. Moreover, the electrochemical signal of MCF-7 cell was stronger than the Hela cell at the same cell concentration, suggesting the miRNA-21 was overexpressed in the cell line of MCF-7 rather than HeLa. Furthermore, the expressed levels of these two cell lines were quantitatively analyzed based on the measured results. In detail, the concentrations of miRNA-21 were 730, 6.65 and 0.15 pM extracted from 10^6, 10^4 and 10^2 MCF-7 cells, respectively while the miRNA-21 of 204, 1.84 and 0.0469 pM respectively for extractions from HeLa cells at the same concentrations as above. The results were agreed with the fact that the miRNA-21 content was positively correlated with the number of cells and consistent with the previously reported articles that the miRNA-21 was highly expressed in MCF-7 than HeLa [25,26], indicating the great potential of our proposed system for quantitative determination or profiling of miRNAs in tumor cells and early diagnosis of diseases.

Preferred position for **Figure 6**

Conclusion

In summary, an ultrasensitive electrochemical biosensor for miRNA-21 analysis was

fully developed via assembling of the multi-branched DNA nanoarchitectures on the electrode surface. In response to miRNA-21, the substantial signal amplification was obtained through the convenient and effective integration of the main body structure of DNA concatamers with the branch structure of G-quadruplex wires, which resulted in a synergistic effect to the amplified electrochemical signal after bound with hemin. With the unique structural merits, the as-prepared electrochemical biosensor allowed the target miRNA-21 to be profiled with a total linear range of 10 fM-100 nM, and the detection limit was 0.2 fM, which also met the biomedical requirements of practical cancer cells analysis. Moreover, even the single-base mutation could be easily distinguished from the target miRNA-21 with this designed electrochemical sensing protocol. It thus potentially opens a promising avenue for versatile amplified sensing platforms construction and holds a promising prospective in the area of DNA based bioanalysis and clinical diagnostics.

Acknowledgments

This work is financially supported by the grant of 2018YFC1603606, 2017YFF0208600, China Agriculture Research System-48 (CARS-48), the special fund of central university 2017HGPA0162, JZ2019HGTB0068, PA2017GDQT0018 and NSFC 21475030, 21804028.

Supporting Information

The Supporting Information is available free of charge on the ACS Publications website at DOI: .

Detailed information of the oligonucleotides sequences, comparison results with other reported biosensors for miRNAs, characterization results of DNA concatamers and G-quadruplex wires and other optimization results (PDF).

References

(1) Zhao, Y.; Srivastava, D. *Trends Biochem. Sci.* **2007**, *32*, 189-197.

(2) Zhang, H.; Li, Y.; Lai, M. *Oncogene* **2010**, *29*, 937-948.

(3) Lu, J.; Getz, G.; Miska, E. A.; Alvarez-Saavedra, E.; Lamb, J.; Peck, D.; Sweet-Cordero, A.; Ebert, B. L.; Mak, R. H.; Ferrando, A. A.; Downing, J. R.; Jacks, T.; Horvitz, H. R.; Golub, T. R. *Nature* **2005**, *435*, 834.

(4) Marabita, F.; Candia, P. D.; Torri, A.; Tegnér, J.; Abrignani, S.; Rossi, R. L. *Brief. Bioinform.* **2016**, *17*, 204-212.

(5) Várallyay, É.; Burgyán, J.; Havelda, Z. *Nat. Protoc.* **2015**, *3*, 190-196.

(6) Li, W.; Ruan, K. *Anal. Bioanal. Chem.* **2009**, *394*, 1117-1124.

(7) Thomson, J. M.; Parker, J.; Perou, C. M.; Hammond, S. M. *Nat. Methods* **2004**, *1*, 47-53.

(8) Cissell, K. A.; Shrestha, S.; Deo, S. K. *Anal. Chem.* **2015**, *79*, 4754-4761.

(9) Mclaughlin, C. K.; Hamblin, G. D.; Sleiman, H. F. *Chem. Soc. Rev.* **2011**, *40*, 5647-5656.

(10) Deng, R.; Zhang, K.; Wang, L.; Ren, X.; Sun, Y.; Li, J. *Chem* **2018**, *4*, 1373-1386.

(11) Nason, M. a. H.; Lea, S.; Tinkara, T.; Wan-Chi, L.; Irena, D.-O.; Mateus, W. d. S. *Chem–Eur. J.* **2014**, *20*, 3626-3630.

(12) Evanko, D. *Nat. Methods* **2004**, *1*, 186-187.

(13) Bi, S.; Yue, S.; Zhang, S. *Chem. Soc. Rev.* **2017**, *46*, 4281-4298.

(14) Liu, B.; Bing, Z.; Chen, G.; Yang, H.; Tang, D. *Biosens. Bioelectron.* **2014**, *53*, 390-398.

(15) Zhang, K.; Lv, S.; Lin, Z.; Tang, D. *Biosens. Bioelectron.* **2017**, *95*, 34-40.

(16) Wu, Y.; Zou, L.; Lei, S.; Yu, Q.; Ye, B. *Biosens. Bioelectron.* **2017**, *97*, 317-324.

(17) Pelossof, G.; Telvered, R.; Willner, I. *Anal. Chem.* **2012**, *84*, 3703-3709.

(18) Xu, J.; Li, H.; Wu, Z. S.; Qian, J.; Xue, C.; Jia, L. *Theranostics* **2016**, *6*, 318-327.

(19) Gao, Z. F.; Huang, Y. L.; Ren, W.; Luo, H. Q.; Li, N. B. *Biosens. Bioelectron.* **2015**, *78*, 351-357.

(20) Kai, S.; Dou, B.; Yang, J.; Yuan, R.; Yun, X. *Biosens. Bioelectron.* **2017**, *87*, 495-500.

(21) Wang, L. J.; Luo, M. L.; Zhang, Q.; Tang, B.; Zhang, C. Y. *Chem. Commun.* **2017**, *53*, 11016-11019.

(22) Lu, L.; Wang, M.; Liu, L. J.; Wong, C. Y.; Leung, C. H.; Ma, D. L. *Chem. Commun.* **2015**, *51*, 9953-9956.

(23) Kumarswamy, R.; Volkmann, I.; Thum, T. *RNA Biol.* **2011**, *8*, 706-713.

(24) Huang, H.; Bai, W.; Dong, C.; Guo, R.; Liu, Z. *Biosens. Bioelectron.* **2015**, *68*, 442-446.

(25) Lu, S.; Wang, S.; Zhao, J.; Sun, J.; Yang, X. *Anal. Chem.* **2017**, *89, 8429-8436*.

(26) Liao, H.; Zhou, Y.; Chai, Y.; Yuan, R. *Biosens. Bioelectron.* **2018**, *114*, 10-14.

Captions of Figures

Figure 1. Schematic diagram of the electrochemical DNA biosensor based on multi-branched DNA nanoarchitectures for amplified electrochemical determination of miRNA-21.

Figure 2. (A) CV and (B) EIS signals of bare Au electrode at different modification stages: (a) bare Au; (b) Au/CP; (c) Au/CP/MCH; (d) Au/CP/MCH/MiRNA-21; (e) Au/CP/MCH/MiRNA-21/DNA concatamers; (f) Au/CP/MCH/MiRNA-21/DNA concatamers/Extended G-quadruplex wires; (g) Au/CP/MCH/MiRNA-21/DNA concatamers/Extended G-quadruplex wires/GUs.

Figure 3. Typical DPV responses corresponding to (a) Au/CP/MCH/DNA concatamers/Extended G-quadruplex wires, (b) Au/CP/MCH/MiRNA-21/DNA concatamers/Extended G-quadruplex wires, (c) Au/CP/MCH/ DNA concatamers/Extended G-quadruplex wires/GUs, and (d) Au/CP/MCH/MiRNA-21/DNA concatamers/Extended G-quadruplex wires/GUs. [miRNA-21]= 100 nM.

Figure 4. (A) DPV measurements of the biosensor to 0, 10 fM, 100 fM, 1 pM, 10 pM, 100 pM, 1 nM, 10 nM, 100 nM, and 500 nM of miRNA-21 (from a to j). (B) The plot of peak current to the target miRNA concentration. Inset: the relationship between the peak current and the logarithm of the target miRNA concentration. The error bars represent the standard deviations of three parallel tests.

Figure 5. Bar graph of relative signal response for sensing electrodes in the presence of T, MT1, MT2, MT3, IM, DM, non-T (MiRNA-10b, MiRNA-141, MiRNA-200b, and Let-7d), and Blank, respectively. The error bars represent the standard deviation of three replicate detections.

Figure 6. Bar graph of signal response for sensing of miRNA-21 from different number of HeLa and MCF-7 cells. The error bars represent the standard deviation of three replicate detections.

Figure 1

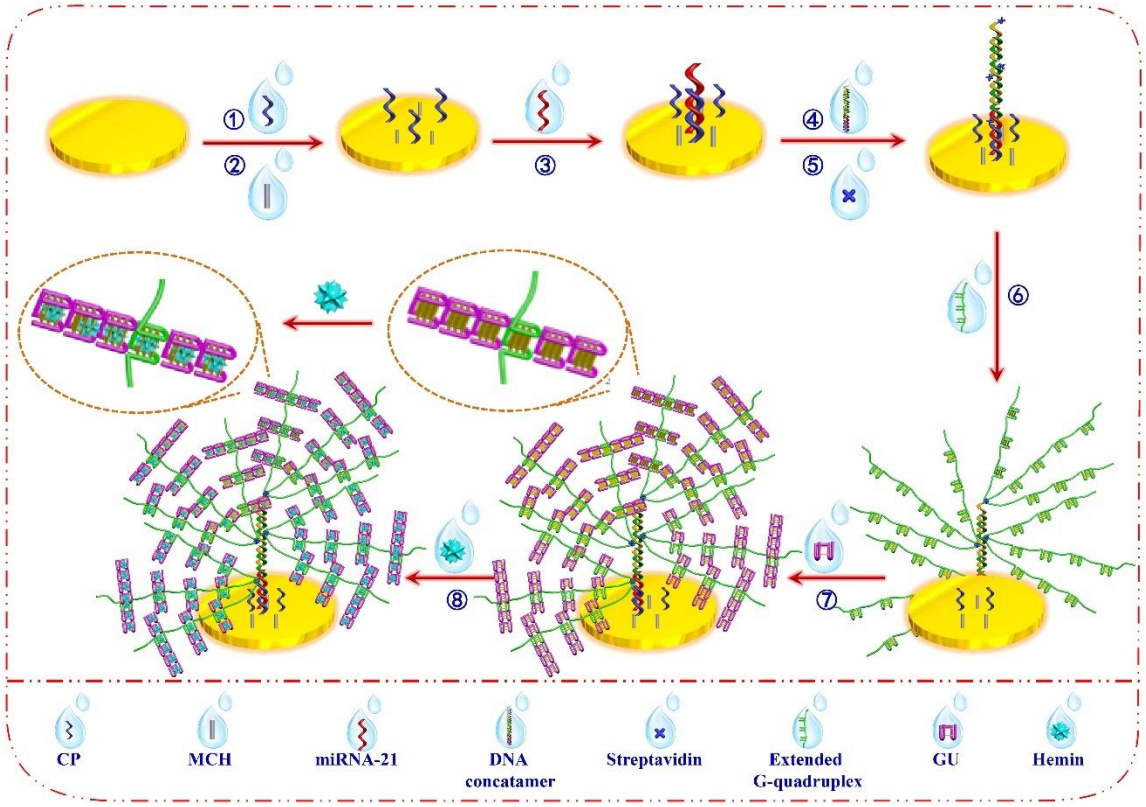
①
②
③
④
⑤
⑥
⑦
⑧
CP
MCH
miRNA-21
DNA concatamer
Streptavidin
Extended G-quadruplex
GU
Hemin

Figure 2

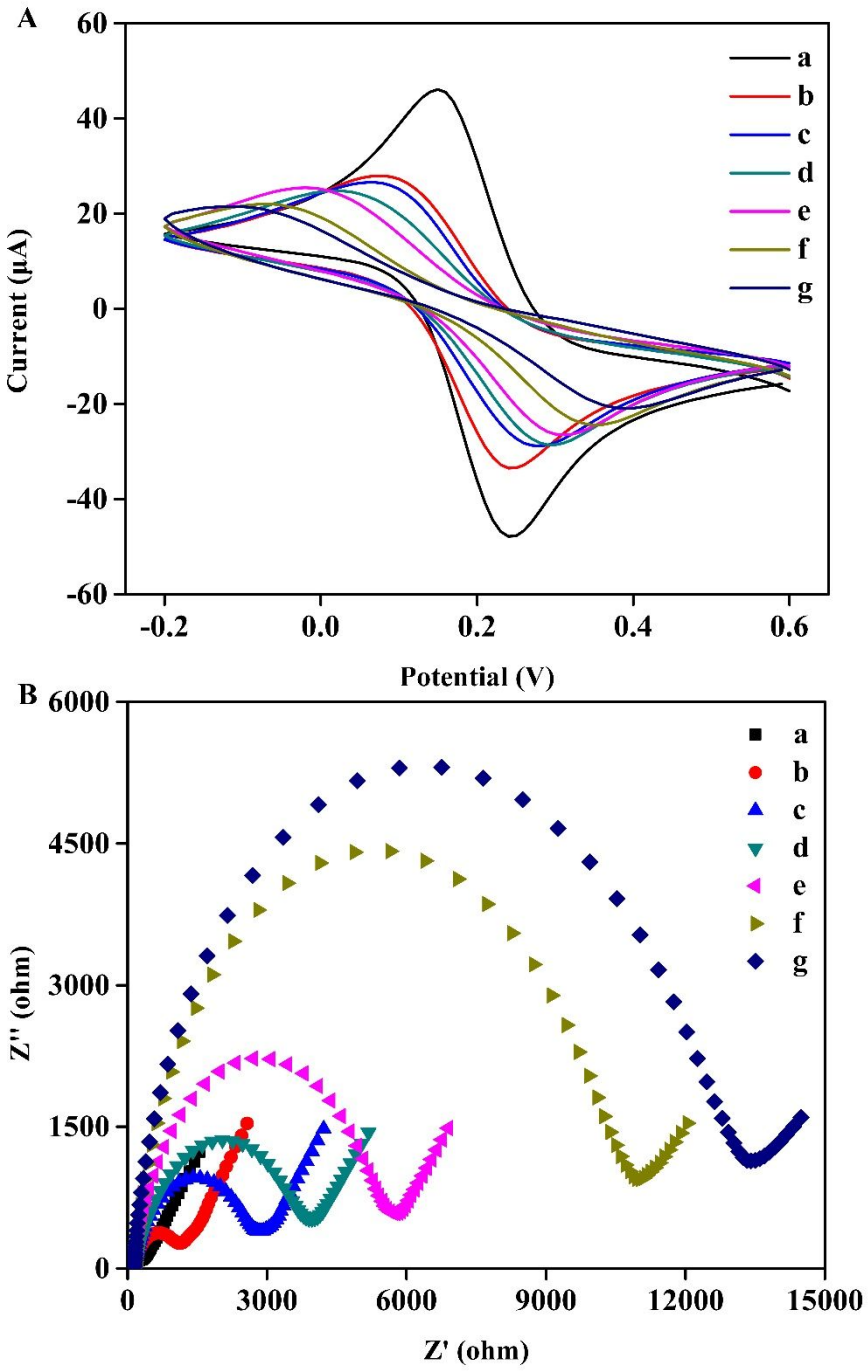

Figure 3

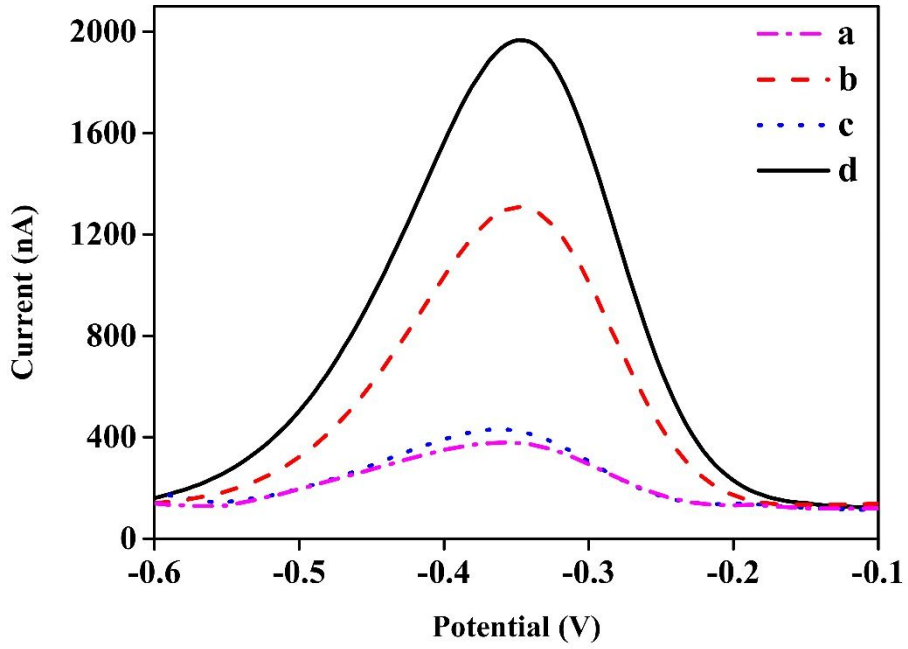
2000
1600
1200
800
400
0
Current (nA)
-0.6
-0.5
-0.4
-0.3
-0.2
-0.1
Potential (V)
a
b
c
d

Figure 4

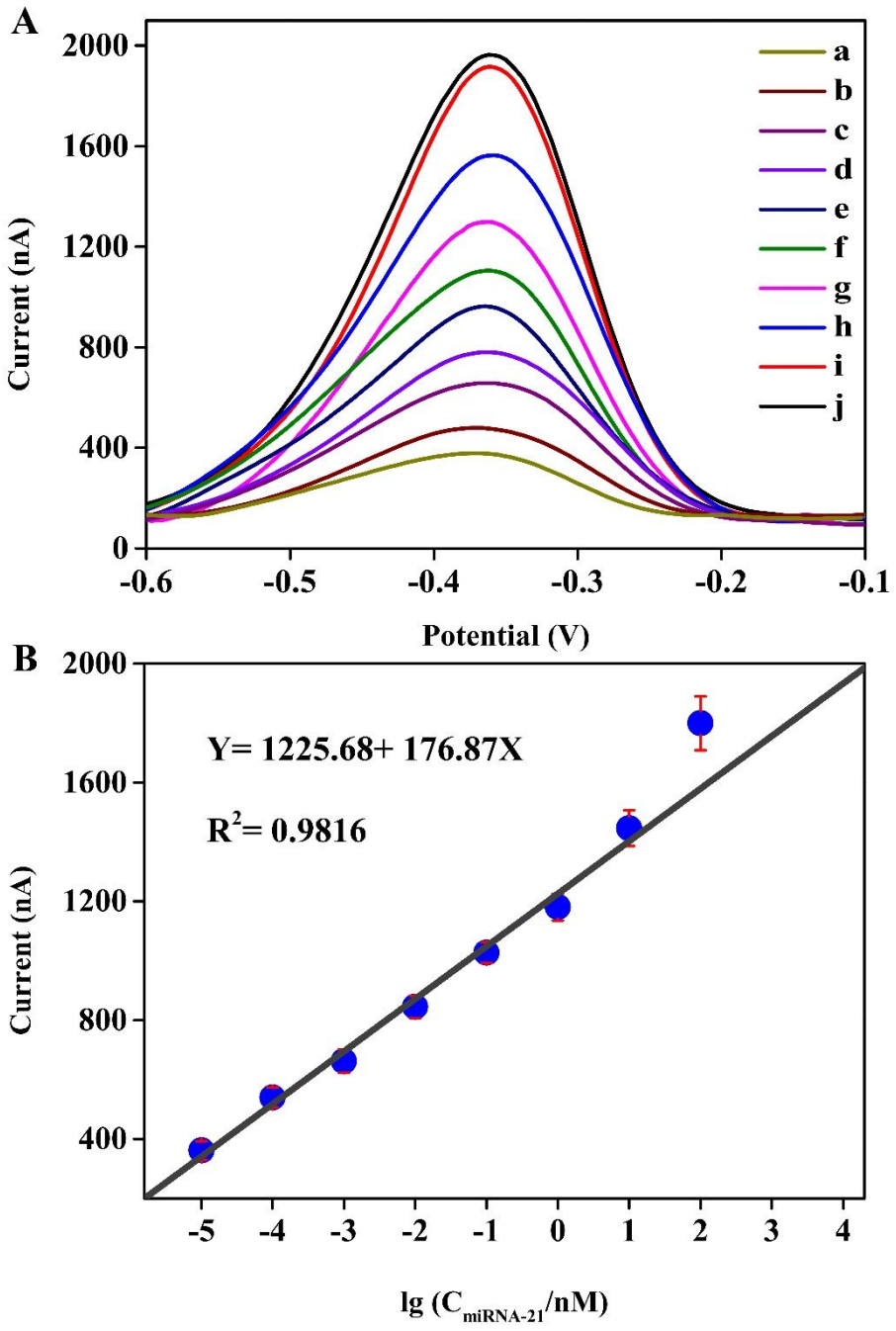
A
Current (nA)
Potential (V)
a
b
c
d
e
f
g
h
i
j
B
Current (nA)
Y= 1225.68+ 176.87X
R²= 0.9816
lg (C miRNA-21/nM)

Figure 5

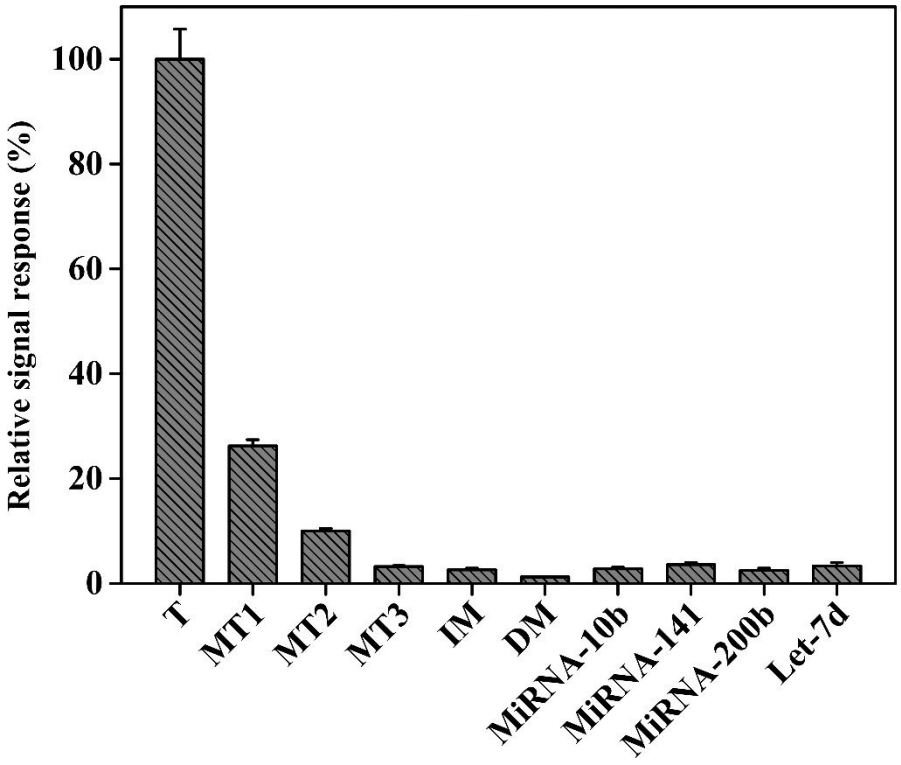
Relative signal response (%)
100
80
60
40
20
0
T
MT1
MT2
MT3
IM
DM
MiRNA-10b
MiRNA-141
MiRNA-200b
Let-7d

Figure 6

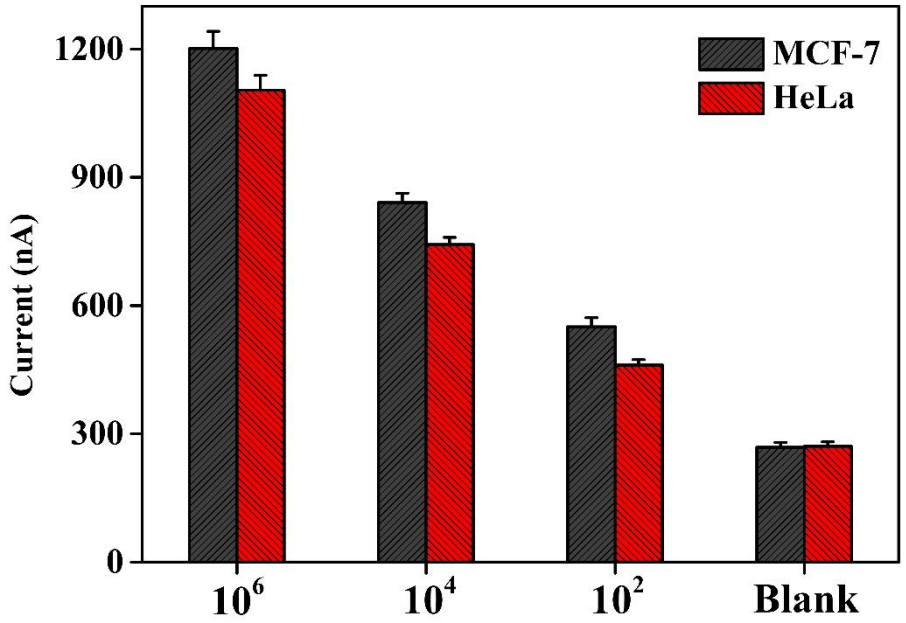

Table of Contents graphic